Supporting Online Material for

Spatial Regulators for Bacterial Cell Division Self-Organize into Surface Waves in Vitro

Martin Loose, Elisabeth Fischer-Friedrich, Jonas Ries, Karsten Kruse,* Petra Schwille*

*To whom correspondence should be addressed. E-mail:
petra.schwille@biotec.tu-dresden.de (P.S.);
k.kruse@physik.uni-saarland.de (K.K.)

This PDF file includes

Materials and Methods
SOM Text
Figs. S1 to S13
Table S1
References

Other Supporting Online Material for this manuscript includes the following:
(available at www.sciencemag.org/cgi/content/full/320/5877/789/DC1)

Movies S1 to S13

Supporting Online Material

S1   Material and Methods

S1.1   Expression and purification of His-MinD

A PCR with primers GCAT<u>GAATTC</u>GCACGCATTATTGTTGTTACTTC and GCGT<u>AAGCT</u>-<u>T</u>TTATCCTCCGAACAAGCGTT was used to amplify a minD-minE fragment from the plasmid pWM1255 (*1*). This fragment was incubated with EcoRI and HinDIII (restrictions sites are underlined) and ligated into similarly treated pET28a to obtain a vector containing minD-minE. The resulting ORF encoded for fusion protein of MinD connected to an N-terminal hexahistidine-tag by a short linker and the sequence for a Thrombin cleavage site and a T7-tag. BL21 cells were transformed with this construct, grown to an OD 600 of 0.6 and induced with 1 mM IPTG for 2-3 hours at 37 °C. Cells were collected by centrifugation and resuspended in lysis buffer (50 mM NaH_2PO_4 pH 7.5, 300 mM NaCl, 10 mM Imidazole, 10 mM β-mercaptoethanol, Protease Inhibitor (Complete EDTA free, Roche Molecular Biochemicals) and 0.2 mM Mg-ADP). After resuspension, cells were lysed by three passages through a Emulsiflex C5 (Avestin). The crude lysate was clarified by centrifugation at 10 000 rpm for 45 min at 4°C and loaded onto a Ni^{2+} sepharose comlumn (NiNTA-superflow, Qiagen). The column was washed with imidazole buffer (50 mM NaH_2PO_4 pH 7.5, 300 mM NaCl, 20 mM imida-

zole, 10 % glycerol, 0.1 mM EDTA, protease inhibitor) and the protein was eluted with elution buffer (50 mM NaH_2PO_4 pH 7.5, 300 mM NaCl, 250 mM imidazole, 10 % glycerol, 0.1 mM EDTA, protease inhibitor). Peak His-MinD fractions were pooled and the buffer exchanged to storage buffer (50 mM HEPES pH 7.25, 150 mM KCl, 10 % glycerol, 0.1 mM EDTA and differents amounts of ADP, depending on protein concentration) by dialysis or PD10 desalting columns (Biorad). His-MinD was stored at -80°C. Protein concentrations were estimated using a Bradford assay (Bio-Rad Protein Assay).

S1.2   Expression and purification of His-MinE and MinE-His

MinE was PCR amplified from the plasmid pWM1255 (*1*) using the primers GCAT<u>GAATTC</u>G-CATTACTCGATTTCTTTCTCTC and GCGT<u>AAGCTT</u>TTATTTCAGCTCTTCTGCTTCC. This fragment was incubated with HinDIII and EcoRI and cloned into similarly treated pET28a to obtain vector with minE seperated from the N-terminal hexahistidine-tag by a short linker and the sequence for a Thrombin cleavage site and a T7-tag. To obtain MinE with a C-terminal hexahistidine tag, we PCR amplified minE from the same plasmid (pWM1255) using the primers GCGT<u>CCATGG</u>CATTACTCGATTTCTTTCTCT and GCGT<u>CTCGAG</u>TTTCAGCTCTTCTG-CTTCC. This fragment was treated with NcoI and XhoI (restriction sites are underlined) and inserted into similar treated pET28a. This resulted in MinE with the peptide sequence EHHH-HHH directly attached to the C-terminus. His-MinE and MinE-His were expressed and purified respectively according to the protocol for His-MinD, but no Mg-ADP was added to the buffers. Both proteins were stored in storage buffer (50 mM HEPES pH 7.25, 150 mM KCl, 10 % glycerol, 0.1 mM EDTA) at -80°C. Protein concentrations were estimated using a Bradford assay (Bio-Rad Protein Assay).

S1.3 Labeling of proteins with fluorescent dyes

Both proteins, MinE and MinD, have only one cystein accessible for labeling with thiol-reactive probes: MinD Cys-52 and MinE Cys-51. Labeling reactions with thiol-reactive dyes were performed according to the protocols of the manufacturer (MinE: Alexa647-maleimide, MinD: Bodipy FL-maleimide, both Molecular Probes). In the case of MinD, an equimolar amount of Mg-ADP was added to the buffer to prevent ATP-dependent dimerization and to screen Cys-119 located close to the ATP-binding site of MinD. We added a 5-fold molar excess of dye to protein and incubated for 2 hours at room temperature. The reaction was quenched with 10mM β-mercaptoethanol and excess dye was separated from the protein by passaging the mixture through a PD10 salt exchange column. Samples were frozen in storage buffer (50 mM HEPES pH 7.25, 150 mM KCl, 10 % glycerol, 0.1 mM EDTA) at -80°C. Average labeling efficiencies for samples used in this study were 80-100 % for MinD and 60-80 % for MinE. After labeling, the activity of both proteins was confirmed in a coupled ATPase assay (see S1.4).

S1.4 ATPase activity assay

To quantify ATP hydrolysis by His-MinD, we used a coupled enzymatic assay (*2*). 5 μM His-MinD and 5 μM His-MinE or 5 μM MinE-His were incubated at 37 °C in the presence of 0.5 mg/ml small unilamellar vesicles of *E. coli* phospholipds, pyruvate kinase (PK, 5 $\mu g/ml$), phosphoenolpyruvate (PEP, 2mM) and ATP (1mM) in 60 μl ATPase buffer (25 mM Tris-HCl pH 7.5, 50 mM KCl, 5 mM MgCl$_2$). At discrete times (after 30 min and 60 min incubation time), we added 20 μl of the reaction mixture to 180 μl of a mixture containing NADH (0.22 mM), LDH (5.56 $\mu g/ml$), PK (0.01 mg/ml) and PEP (2.22 mM) and the absorption of light at 340 nm was observed in a spectrophotomer (Analytik Jena Specord S 100). The amount of ATP hydrolyzed by MinD was calculated from changes in A$_{340}$ (NADH) ($\epsilon = 6220 M^{-1} cm^{-1}$)

compared to a control containing no Min proteins.

S1.5 Self-organization assay

The reaction chamber for the self-organization assay was prepared by attaching a plastic ring on a cleaned glass cover slip. Freshly cleaved mica was glued on the bottom of the chamber (see Fig. S2). For supported lipid bilayer formation, SUVs (small unilamellar vesicles) were prepared by sonication at room temperature from *E. coli* polar lipid extracts (Avanti Polar Lipids, Alabaster, AL) at 4 mg/ml and 0.1 mol % DiIC-C18 or DiD in reaction buffer (25mM Tris-HCl pH 7.5, 150mM KCl, 5 mM $MgCl_2$). The SUV suspension was diluted in reaction buffer to 0.5 mg/ml and added to the reaction chamber. Adding $CaCl_2$ to a final concentration of 0.1 mM induced fusion of the vesicles and the formation of a lipid bilayer on the mica surface. After 10 min of incubation at 37°C, the sample was rinsed with 2 ml warm reaction buffer. Before each experiment, the integrity of the membrane was confirmed by FRAP experiments. For the self-organization assay, 2.5 mM ATP and an ATP-regenerating system (4 mM phospho-enolpyruvate and 0.01 μ g/ml pyrovate kinase) were added to the reaction buffer. MinD, doped with 20% MinD-Bodipy-FL, and MinE, doped with 10 % MinE-Alexa647, were successively added (within 5 min) to the reaction chamber and incubated at 20°C. The order of additions did not change the final pattern. The final volume of the assay was usually 200 μl. The reaction chamber was closed with a lid of a Eppendorf reaction tube during observation.

S1.6 Imaging

Confocal imaging was performed using a Zeiss LSM 510 microscope with a Zeiss C-Apochromat 40x, NA=0.75 water immersion objective at 20°C. The laser power was adjusted depending on the available signal intensity under different experimental conditions. Therefore, fluorescence

intensities are not directly comparable between experiments. The fluorescence signal was detected with a photomultiplier.

S1.7 Image analysis

Image processing and analysis was carried out with Image J (Rasband, W.S., ImageJ, U. S. National Institutes of Health, Bethesda, Maryland, USA, http://rsb.info.nih.gov/ij/, 1997-2007).

S1.8 Photobleaching experiments and FRAP measurements

Self-organization experiments were performed as explained in section S1.5 with an oxygen scavenger system (40 mM D-glucose, 0.040 mg/ml glucose oxidase, 0.016 mg/ml catalase, and 20 mM DTT) added to the buffer. Surface waves were visualized with a Zeiss LSM 510 confocal microscope. After the final pattern had formed, a rectangular area of MinD-Bodipy or MinE-Alexa647 within the travelling protein band was bleached with 10 iterations (see Fig. S9A and S10A).

Fluorescence recovery after bleaching can occur through two overlying processes: 2D-diffusion of proteins attached to the membrane and exchange of membrane-bound proteins with proteins in the buffer. In order to analyze recovery of the bleached area in Fig. S9A and S10A due to diffusion in the plane of the membrane, we made two assumptions: First, that chemical and physical properties of the proteins were not modified by bleaching of the dye and second, that the protein densities were approximately homogenous parallel to the travelling protein band. Thus, the smearing out of the box-shaped bleaching profile along the thick line shown in Fig. S9 A and S10 A was due to diffusion of membrane-bound MinD and MinD-MinE, respectively. Solving the diffusion equation in 1D with an initial square well concentration gives $I(x, t) = A(1 - \frac{1}{2}(\mathrm{erf}(\frac{x - x_1}{\sigma}) + \mathrm{erf}(\frac{x_2 - x}{\sigma}))) + B$, where erf denotes the Gaussian error function and $\sigma =$

$\sqrt{4Dt}$. We fitted this function to the intensity profile plot along the rectangular area in Fig. S9 A and S10 A for each frame of the movie using a custom written Matlab macro. The flattening of the function $I(x,t)$ with time was then caused by the diffusion of bleached molecules out of the bleached area and by the diffusion of non-bleached molecules into the bleached area (*3*).

Intensities were averaged over the width of the line to reduce noise and the height of the well was given by A and the background level by B. The constants x_1 and x_2 were obtained from the intensity profile at time zero after bleaching. The remaining parameters A, B and σ were fitted for each time individually (see Fig. S9 B-D and S10 B-D). The linear function $\sigma^2 = 4Dt$ was fitted to the plot of σ^2 versus time and from the slope of this function we determined the diffusion constants D_d and D_{de} (see Fig. S9 E and S10 E). These values correspond to the translational movement of the respective fastest protein species, e.g. in the case of D_d we assumed the translational movement of slow MinD-MinE complexes to be superimposed by the fast movement of MinD alone. It should be noted that the measured values are effective diffusion constants which might not only result from Brownian motion.

S1.9 FCS measurements

The diffusion constant of the labeled proteins in solution (1 nM MinD-Alexa488 and 1 nM MinE-Alexa647 in 25mM Tris-HCl pH 7.5, 150mM KCl, 5 mM $MgCl_2$) were obtained by Fluorescence Correlation Spectroscopy (FCS) performed on a commercial ConfoCor 3 combination system (Carl Zeiss). Correlation curves $G(\tau)$ were fitted appropriately by the FCS model equation for three-dimensional free Brownian diffusion according to published literature (*4*) (see Fig. S8).

S2   Supplementary Movies

Movie S1: Movie of Min protein waves. MinD (1 μM), doped with 20% Bodipy-labeled MinD (green), MinE (1 μM), doped with 10% Alexa647-labeled MinE (red). Scale bar is 50 μm, frames are 9 sec apart.

Movie S2: Movie of Min protein waves, scale bar is 50 μm, frames are 13 sec apart. MinD (1 μM), doped with 20% Bodipy-labeled MinD (green), MinE (1.5 μM), doped with 10% Alexa647-labeled MinE (red).

Movie S3: Example of protein dynamics in the presence of 0.125 μM MinE, doped with 10% Alexa647-labeled MinE (red) and 1 μM MinD, doped with 20% Bodipy-labeled MinD (green). Scale bar is 50 μm, frames are 18 sec apart.

Movie S4: Movie of initiation of Min protein waves. MinD (1 μM), doped with 20% Bodipy-labeled MinD (green), MinE (1 μM), doped with 10% Alexa647-labeled MinE (red). Scale bar is 20 μm, frames are 23 sec apart.

Movie S5: Movie of synchronization of Min protein waves. MinD (1 μM), doped with 20% Bodipy-labeled MinD (green), MinE (1 μM), doped with 10% Alexa647-labeled MinE (red). Scale bar is 50 μm, frames are 13 sec apart. MinD (green), MinE (red).

Movie S6: Movie of a spiral of Min proteins. MinD (1 μM), MinE (1 μM), doped with 10% Alexa647-labeled MinE. Scale bar is 100 μm, frames are 14 sec apart.

Movie S7: Movie of a spiral of Min proteins. MinD (1 μM), doped with 20% Bodipy-labeled MinD (green), MinE (1 μM), doped with 10% Alexa647-labeled MinE (red). Scale bar is 50 μm, frames are 10 sec apart.

Movie S8: Movie of a spiral of Min proteins. MinD (1 μM), doped with 20% Bodipy-labeled MinD (green), MinE (1 μM). Scale bar is 50 μm, frames are 9 sec apart.

Movie S9: Movie of a double spiral of Min proteins. MinD (1 μM), MinE (0.5 μM), doped

with 10% Alexa647-labeled MinE. Scale bar is 50 μm, frames are 14 sec apart.

Movie S10 A: Simulation of Min protein dynamics. The MinD is shown in green, MinE in red. This movie corresponds to Fig.4A in the article. The concentrations range for MinD from 0 to $\sim 6 \cdot 10^6 \mu m^{-2}$, and for MinE from 0 to $\sim 5.4 \cdot 10^6 \mu m^{-2}$. In total a square of side length $900 \mu m$ is shown, for a period of 14.5 minutes.

Movie S10 B: Extract of Movie S10 corresponding to the area shown in Fig.4A in the article. The square has a side length of $400 \mu m$.

Movie S11: Simulation of Min protein dynamics. Only MinE is shown. This movie corresponds to Fig.4D in the article. The parameters are as in Movie S10 but different initial concentrations have been chosen. The concentration range equals the one in Movie S10. Shown is a square of side length $540 \mu m$ for a period of 11.5 minutes.

Movie S12 A: Simulation of Min protein dynamics according to the Min-oscillation model presented in (5). Color coding is as in Movie S10. In total, a square of $900 \mu m$ has been simulated with periodic boundary conditions. Shown is a patch of $600 \mu m$ side length covering 4 minutes. The total concentration of MinD in the system was $1 \mu M$, and of MinE $0.34 \mu M$. The remaining parameters were $\sigma_{de} = 0.67 s^{-1}, \sigma_D = 0.17 s^{-1}, \sigma_{dD} = 2.6 \cdot 10^{-7} \mu m^2/s, \sigma_E = 1.5 \cdot 10^{-5} \mu m^2/s, D_D = D_E = 60 \mu m^2/s, c_{\max} = 12.6 \cdot 10^6 \mu m^{-2}$. The exchange of ADP for ATP in unbound MinD was assumed to be instantaneous. The use of a finite exchange rate did not give qualitative changes. The concentrations range for MinD from 0 to $\sim 12 \cdot 10^6 \mu m^{-2}$, and for MinE from 0 to $\sim 3.8 \cdot 10^6 \mu m^{-2}$.

Movie S12 B: Simulation of the model presented in (5). In total, a square of $450 \mu m$ has been simulated with periodic boundary conditions. The movie covers 1 minute. The total concentration of MinD in the system was $1 \mu M$, and of MinE $0.35 \mu M$. The remaining parameters were $\sigma_{de} = 0.7 s^{-1}, \sigma_{ADP \to ATP} = 1 s^{-1}, \sigma_D = 0.098 s^{-1}, \sigma_{dD} = 6.6 \cdot 10^{-7} \mu m^2/s, \sigma_E = 4 \cdot 10^{-5} \mu m^2/s, D_D = D_E = 63 \mu m^2/s, c_{\max} = 18.75 \cdot 10^6 \mu m^{-2}$. The concentrations range for

MinD from 0 to $\sim 17.25 \cdot 10^6 \mu m^{-2}$, and for MinE from 0 to $\sim 7.5 \cdot 10^6 \mu m^{-2}$.

Movie S13: Simulation of Min protein dynamics according to the Min-oscillation model presented in (*6*). Color coding is as in Movie S10. Shown is a square of $250 \mu m$ side length covering 20 minutes simulated with periodic boundary conditions. The total concentration of MinD in the system was $1 \mu M$, and for MinE $1 \mu M$. The remaining parameters were $\sigma_{de} = 0.002 s^{-1}, \sigma_D = 0.0004 s^{-1}, \sigma_E = 3.3 \cdot 10^{-9} \mu m^2 / s, c_{\max} = 6 \cdot 10^6 \mu m^{-2}$. The concentrations range for MinD from 0 to $\sim 1 \cdot 10^6 \mu m^{-2}$, and for MinE from 0 to $\sim 6 \cdot 10^5 \mu m^{-2}$. The buffer proteins were assumed to be well-stirred, i.e. spatial variations of the concentrations within the buffer were negelected.

S3 Supplementary Figure Legends

Figure S1: MinD ATPase assays. The graph shows ATPase activity of His-MinD and His-MinD-Bodipy-FL (MinD*) in the presence of phospholipids. Labeled and unlabeled showed similar rates in the absence of MinE. His-MinE (H-MinE), MinE-His (MinE-H) and His-MinE-Alexa647 (H-MinE*) stimulated the ATPase activity of MinD to a similar degree. Asterisks indicate that fluorescently labeled protein was used.

Figure S2: (A) Schematic diagram of the in vitro assay. A lipid bilayer, which mimicked the cell membrane, was formed on a freshly cleaved mica surface glued to a glass cover slide. ATP and the proteins MinD and MinE were successively added to the buffer. Laser scanning confocal microscopy was used to observe the labeled molecules. (B) Diagram of the MinD/MinE reaction cycle: (I) ATP-bound MinD dimerizes and attaches to the membrane (II). There, MinE dimers bind to membrane-bound MinD and induce its ATPase activity (III). Upon hydrolysis of ATP, MinD detaches from the membrane and dissociates into monomers (IV). MinD has to undergo nucleotide exchange, before it can rebind to the membrane, MinD needs to exchange

the nucleotide (V).

Figure S3: MinE-His gave the same pattern as His-MinE. Confocal images of Min proteins waves on the lipid membrane. MinD (1 μM) was doped with 20 % Bodipy-labeled MinD (left), MinE-His (1.7 μM) with 10 % Alexa647-label MinE-His (middle) and overlay (right). Below: Profile plots for MinD and MinE and kymograph along the rectangular area shown in the micrographs and kymograph of MinD-MinE waves. Surface wave velocity calculated from the kymograph was 0.45 $\mu m/s$.

Figure S4: Higher concentrations of labeled proteins did not have an observable effect on the surface waves. (A) Surface waves with 80 % of MinE labeled with Alexa647 (MinD = MinE = 1 μM). (B) Surface waves with 40 % of MinD labeled with Bodipy-FL (MinD = MinE = 1 μM). Scale bar = 50 μm.

Figure S5: Protein binding and pattern formation did not have an observable effect on the supported membrane. Red, membrane labeled with 0.1 mol % DiC18. Green, MinD (1 μM) doped with 20 % Bodipy-labeled MinD, MinE (1 μM) was not labeled. Scale bar = 50 μm.

Figure S6: Wave formation depends on ATP hydrolysis. In the presence of 1.25 mM ATPγS, no waves were observed after more than 2 hours of incubation. MinE (1 μM), doped with 10% Alexa647-labeled MinE (red, left), MinD (1 μM), doped with 20% Bodipy-labeled MinD (green, middle) and overlay (right). Scale bar = 50 μm.

Figure S7: Wave formation did not depend on the concentration of ATP . Similar patterns of MinD and MinE were found at varying concentrations of ATP (0.05 to 0.5 mM). MinE (1 μM), doped with 10% Alexa647-labeled MinE (red, left), MinD (1 μM), doped with 20% Bodipy-labeled MinD. Scale bar = 50 μm.

Figure S8: Fluorescence spectroscopy measurements of MinD-Alexa488 and MinE-Alexa647. The graphs show autocorrelation curves and corresponding fits.

Figure S9: Photobleaching and FRAP experiments for MinD bound to the membrane: (A)

Wave propagation was not associated with protein transport on the membrane. Sequential frames of photobleaching experiment (MinD (1 μM, doped with 20% Bodipy-labeled MinD) and MinE (1 μM)). Scale bar = 20 μm. (B) & (C) Intensity profile along the rectangular line in (A) after 1.6s and 16s after bleaching and corresponding fit. (D) Overlay of the two normalized fitted curves from (B) and (C). (E) Mean square displacement plot of the values of $\sigma(t)^2$ obtained from the fitted curves from (B) and (C).

Figure S10: Photobleaching and FRAP experiments for MinDE complexes bound to the membrane: (A) Wave propagation was not associated with protein transport on the membrane. Sequential frames of photobleaching experiment (MinD (1 μM) and MinE (1 μM, doped with 10% Alexa647-labeled MinE)). Scale bar = 20 μm. (B) & (C) Intensity profile along the rectangular line in (A) after 3.2s and 25.6s after bleaching and corresponding fit. (D) Overlay of the two normalized fitted curves from (B) and (C). (E) Mean square displacement plot of the values of $\sigma(t)^2$ obtained from the fitted curves from (B) and (C).

Figure S11: Example of pattern formation at high concentrations of MinD. MinD (1.5 μM) was doped with 20 % Bodipy-labeled MinD (green), MinE (1 μM) with 10 % Alexa647-label MinE (red).

Figure S12: Surface waves of Min proteins reformed from static patterns in presence of MinE concentrations higher than 1.5 μM. MinD (1.5 μM) was doped with 20 % Bodipy-labeled MinD (green), intial concentration of MinE was 1 μM, after static pattern had formed, the concentration was increased to 3 μM (at time = 0 min) (doped with 10% Alexa647-labeled MinE, red). Scale bar = 50 μm.

Figure S13: Example of pattern formation in the cell according to the equations (1)-(4). The oscillation period is 67s. The overall MinD and MinE concentration was set to $1000 \mu m^{-1}$ and $400 \mu m^{-1}$, respectively. The cell length is $2 \mu m$. The remaining parameter values are $\omega_{de} = 0.125 s^{-1}, \omega_D = 0.0013 s^{-1}, \omega_{dD} = 9.3 \cdot 10^{-4} \mu m/s, \omega_E = 3.8 \cdot 10^{-5} \mu m/s, \omega_{eE} =$

$8 \cdot 10^{-9} \mu m^3/s, D_D = D_E = 12.5 \mu m^2/s, D_d = D_{de} = 0.013 \mu m^2/s$. For simplicity, we used the same cytoplasmic diffusion constants for MinD and MinE. The respective values are motivated by Meacci *et al.* (*7*).

S4 Supplementary text

S4.1 The theoretical model

The state of the system is described by the densities of c_D and c_E for the distributions of MinD and MinE in the buffer/cytosol, along with c_d and c_{de} for MinD and MinD/MinE complexes on the membrane. The time evolution of the concentrations is given by the dynamic equations

$$\partial_t c_D = \omega_{de} c_{de} - c_D(\omega_D + \omega_{dD} c_d) + D_D \triangle c_D \tag{1}$$

$$\partial_t c_E = \omega_{de} c_{de} - c_E c_d(\omega_E + \omega_{eE} c_{de}^2) + D_E \triangle c_E \tag{2}$$

$$\partial_t c_d = c_D(\omega_D + \omega_{dD} c_d) - c_E c_d(\omega_E + \omega_{eE} c_{de}^2) + D_d \triangle c_d \tag{3}$$

$$\partial_t c_{de} = c_E c_d(\omega_E + \omega_{eE} c_{de}^2) - \omega_{de} c_{de} + D_{de} \triangle c_{de} \tag{4}$$

Diffusive transport of the proteins is captured by the last terms in the equations, where $\triangle$ is the Laplace operator. The respective attachment/detachment dynamics is parametrized by $\omega_D, \omega_{dD}, \omega_E, \omega_{eE}$ and ω_{de}. The first terms in Eqs.(1)-(2) describe unbinding of MinD/MinE complexes from the membrane. The appearance of this term with a minus-sign in Eq.(4) assures that no material is lost or generated during this process. The second term in Eq.(1) describes binding of MinD to the membrane, with an effective rate that increases with higher concentrations of membrane-bound MinD. The second term in Eq.(2) accounts for cooperative binding of MinE to membrane-bound MinD. The effective attachment rate increases with the number of membrane-bound MinD/MinE complexes. The same term appears in Eq.(3) since

membrane-bound MinD is transformed during MinE binding into a bound MinD/MinE complex. We assume that the exchange of ADP for ATP in unbound MinD is so fast that we do not have to consider explicitly the concentrations of MinD bound to ADP. For each rate, we used only the terms with the lowest order non-linearity that were sufficient to reproduce the phenomena observed experimentally. All the parameters are effective parameters and might account for multiple processes.

Note, that while the densities of MinD and MinE in the buffer are volume concentrations, the densities c_D and c_E in Eqs. (1)-(4) are taken as two-dimensional surface densities. To transform the actual protein concentrations in the buffer into 2D surface densities used in Eqs. (1)-(4), we multiply the volume concentrations by the height of the buffer. This is appropriate if the volume concentrations do not depend on the distance from the membrane. Since mixing of the buffer (using normal micropipettes) did not have an effect on the protein pattern on the membrane, the dependence of the protein concentrations on the distance to the membrane can be neglected. Diffusion in the buffer is by orders of magnitude larger than on the membrane. The values of the diffusion constants influence the characteristic size of the developing pattern, which scales roughly like the square root of D.

S4.2 Numerical solution of the dynamic equations

Equations (1)-(4) have been solved numerically using a forward Euler discretization scheme for the time step. The 2D simulations of the in vitro dynamics have been carried out for a square with side lengths of $900\mu m$, using periodic boundary conditions and a spatial grid with lattice spacing of $7.5\mu m$, or smaller. Simulations with smaller grid sizes did not exhibit qualitative differences. The time step was chosen as $\triangle t = 0.01s$.

Simulations were performed in two spatial dimensions. Protein concentrations in the buffer, as taken from the experiment, were converted to 2D surface densities for the simulations by

multiplying with the height of the buffer ($5mm$). Thus, $1\mu M$ corresponds to a surface density of $3 \cdot 10^6$ particles per μm^2. The parameters chosen for the solutions shown in Fig.4 of the main text are given in Tab. S1.

Membrane detachment rate of MinD-MinE complexes	$\omega_{de} =$	$0.029s^{-1}$
Membrane attachment rate of MinD-ATP	$\omega_D =$	$2.9 \cdot 10^{-4}s^{-1}$
Binding cooperativity coefficient MinD-ATP	$\omega_{dD} =$	$4.8 \cdot 10^{-8}\mu m^2/s$
Attachment rate of MinE to membrane bound MinD-ATP	$\omega_E =$	$1.9 \cdot 10^{-9}\mu m^2/s$
Binding cooperativity coefficient of MinE	$\omega_{eE} =$	$2.1 \cdot 10^{-20}\mu m^6/s$
Diffusion constant of MinD and MinE in buffer	$D_D = D_E =$	$60\mu m^2/s$
Diffusion constant of MinD on membrane	$D_d =$	$1.2\mu m^2/s$
Diffusion constant of MinD-MinE complexes on membrane	$D_{de} =$	$0.4\mu m^2/s$

Table S1: Parameters chosen for the solutions of the model

Diffusions constants of both proteins (D_D, D_E, D_d and D_{de}) were estimated by FRAP and FCS measurements. Using FCS we obtained D_D = 61.32 $\pm$ 1.98 $\mu m^2/s$ and D_E = 58.71 $\pm$ 2.85 $\mu m^2/s$ (see S1.9 and Fig. S8), by FRAP we measured D_d = 0.94 $\mu m^2/s\pm50\%$ (SD) and D_{de} = 0.19 $\mu m^2/s\pm50\%$ (SD) (see S1.8, Fig. S9 and Fig. S10). These values are apparent diffusion constants and might also depend on the kinetics of protein attachment/detachment. Lower values for D_{de} compared to D_d can be explained with higher-order complexes of MinE, which is compatible with the observation of MinE cooperativity. For the parameter values given in Tab. S1, different values for the diffusion constant D_{de} have been tested. In the range from $0.5\mu m^2/s$ to $0.1\mu m^2/s$ the results of the simulations were qualitatively similar. We numerically solved the dynamic equations also for a bacterial geometry, where we used lower values for the diffusion constants of the membrane bound proteins according to (7). We assumed the pattern to be invariant with respect to rotations around the bacterium's long axis, which lead to an effectively one-dimensional system. We have used a 1D spatial grid with lattice spacing of $0.2\mu m$. The time step was $\triangle t = 0.00003s$. The resulting dynamics is shown in Fig. S13 and clearly reveals the pole-to-pole oscillations typical for the Min-proteins in *E. coli*.

S4.3 Activity of proteins

MinD binds to the membrane via a C-terminal amphipathic helix. We used N-terminally His-tagged MinD (His-MinD) to allow proper membrane binding. The functionality of His-MinD in vivo has been demonstrated by Lackner *et al.* (*8*). MinE interacts with MinD via an N-terminal α-helix activating the ATPase activity of MinD (*9*). The C-terminal domain of MinE is responsible for homodimerization of MinE (*10*) and the formation of the E-ring in vivo (*11*), suggesting that it plays an important role during MinE-MinE interactions. Since both domains seem to have important functions for Min protein dynamics, we decided to purify and test both, C- and N-terminally His-tagged MinE, for their ability to self-organize together with His-MinD in vitro.

First, we checked for the ATPase activity of MinD and the ability MinE to stimulate MinD. We found a basal His-MinD ATPase rate of 0.23×10^{-2} s^{-1} in the absence of MinE and a 12-fold increase to 2.8×10^{-2} s^{-1} when C-terminally His-tagged MinE (MinE-His) was added. When N-terminally His-tagged MinE (His-MinE) was used, we could also observe stimulation of the MinD ATPase activity to a slightly higher rate of 3.7×10^{-2} s^{-1} (16 fold) (see Fig. S1). From these results we concluded that both proteins, N- and C-terminally tagged MinE, are able to bind and activate MinD in vitro.

We also tested the activity of the fluorescently labeled proteins: The ATPase rate of Bodipy-labeled MinD (=MinD*) was slightly lower (3.0×10^{-2} s^{-1}) compared to the unlabeled protein. Alexa-labeled MinE (MinE*) stimulated the ATPase activity of MinD to a similar degree ($\sim$12 fold to 2.7×10^{-2} s^{-1}) as unlabeled MinE.

The values of the MinD ATPase rate in the presence of MinE were similar to corresponding values already published. These values range broadly from 4.8×10^{-3} s^{-1} to 5.5×10^{-2} s^{-1} (*8, 12–16*). This broad range might be due to different vesicle preparation methods, lipid composition, age of the lipids and size of the vesicles used.

In our self-organization assay, both versions of MinE (His-MinE and MinE-His) were able to form dynamic patterns in vitro. Since initial results had shown that cooperativity during MinE binding to MinD-MinE complexes on the membrane was important, we decided to use N-terminally His-tagged MinE for the following experiments. Nevertheless, MinE-His was also able to form surface waves and the protein bands also showed the same protein distribution as His-MinE (Fig. S3).

Furthermore, the pattern was not influenced by using Min proteins where the His-tag had been removed by Thrombin digestion (Thrombin Kit, Novagen, protocol according to the manufacturer). Also when we used labeled MinD and unlabeled MinE or vice versa, the pattern did not change. Varying ratios of labeled to unlabeled protein (MinD: 5-40 %, MinE: 5-80 %) did not have an observable effect on the surface waves This confirmed that fluorescence-labeling did not influence pattern formation (see Fig. S4).

S4.4   Surface waves at low concentrations of ATP

The model by Huang *et al.* proposed that the nucleotide exchange rate of MinD was an important parameter during Min oscillations and that nucleotide exchange occured with a finite velocity (*5*). In order to test if the nucleotide exchange rate plays an important role, we performed self-organization experiments at varying ATP concentrations. Also at very low ATP concentrations (0.05 - 0.5 mM), Min proteins still formed similar patterns on the membrane in vitro as at high ATP concentration (2.5 mM) (see Fig. S7), suggesting that the rate of nucleotide exchange does not have a large influence on Min protein pattern formation.

S4.5   Formation of static patterns of Min proteins and the role of MinD polymers

Previous in vitro studies have shown that above a critical concentration, MinD is able to deform lipid vesicles into tubes (*13*). EM micrographs revealed that in this case MinD assembled into polymers on the lipid membrane, but the role of MinD polymerization during Min oscillations is unknown.

During normal wave formation, we did not observe MinD polymers at MinD concentrations of 1 μM and lower. However, for MinD concentrations higher than 1.25 μM and MinE concentrations lower than 2 μM, we found MinD to form filaments on the membrane, which were surrounded by a thin line of MinE (Fig. S11). This pattern was static and did not change during the time of observation ($>$ 30 min). When we increased MinE concentrations to a value higher than 2 μM, the static structures dissolved and surface waves formed (Fig. S12).

The static strands of MinD might represent mesoscopic polymer structures related to the MinD polymers observed by EM in vitro (*13*). The stationary behaviour of the Min proteins was qualitatively different to the dynamic surfaces waves we observed at low MinD concentrations and therefore not captured by our model.

Since the static pattern of Min proteins formed reversibly, similar MinD strands could also form transiently in vivo, when local MinD densities on the membrane are high and before MinE dissolves the static filaments. Transient filament formation at high MinD densities could be the explanation for the dynamic MinD polymers observed in vivo (*17*).

# S5   Supplementary Figures

Figure S1:
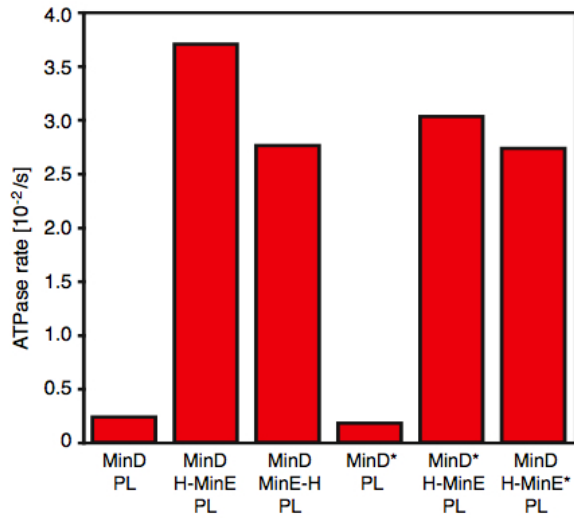

Figure S2:
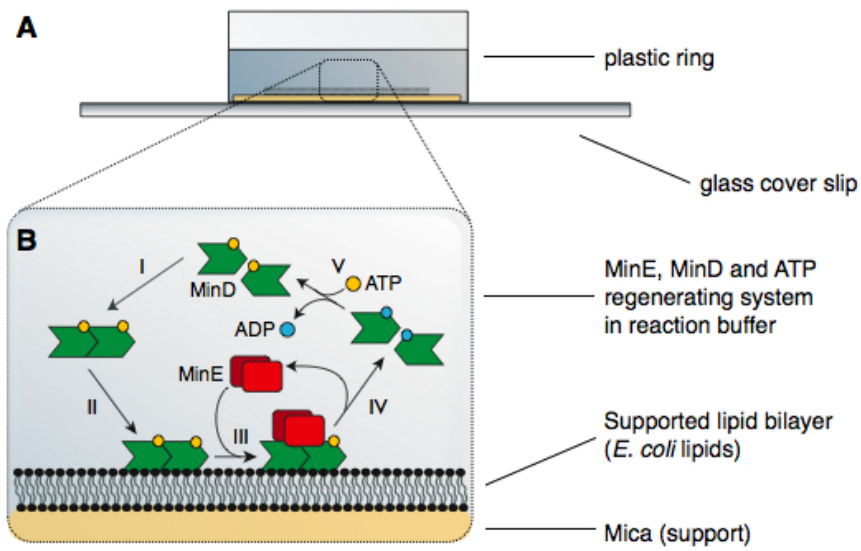
Figure S3:
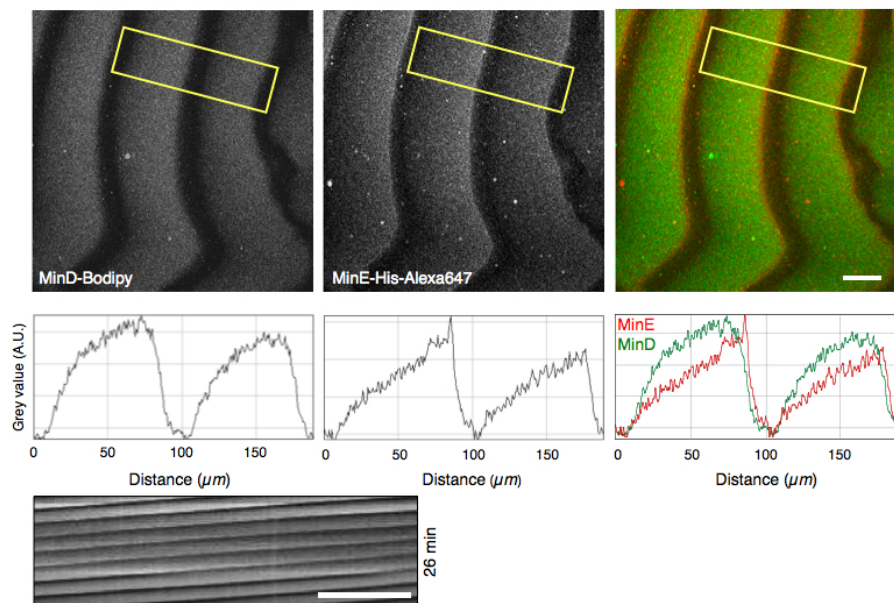

Figure S4:
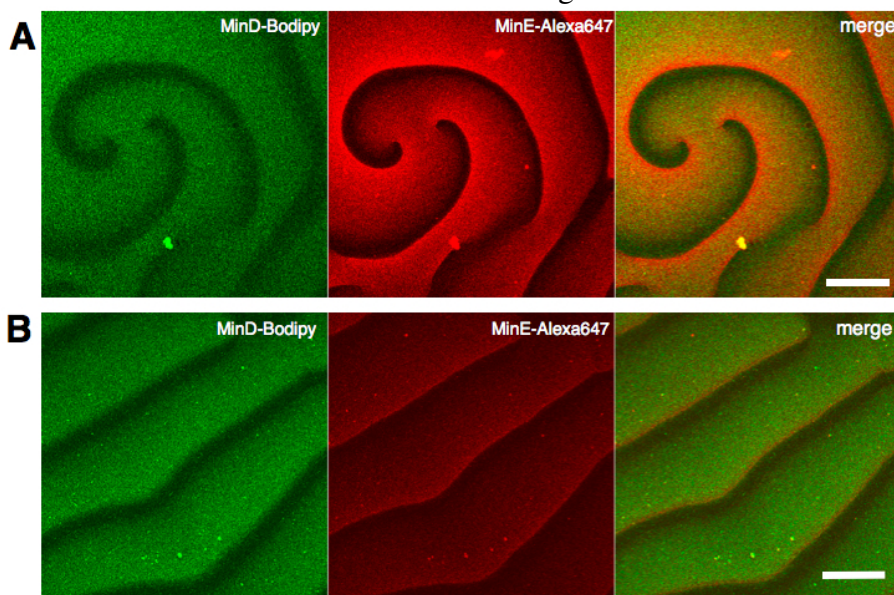
Figure S5:
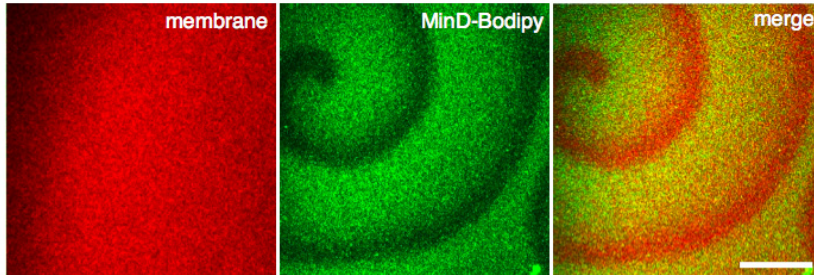
Figure S6:
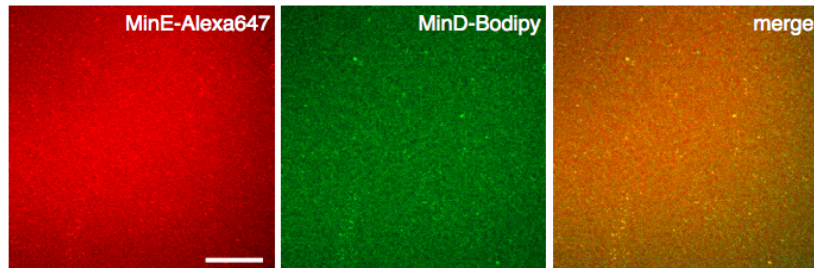
Figure S7:
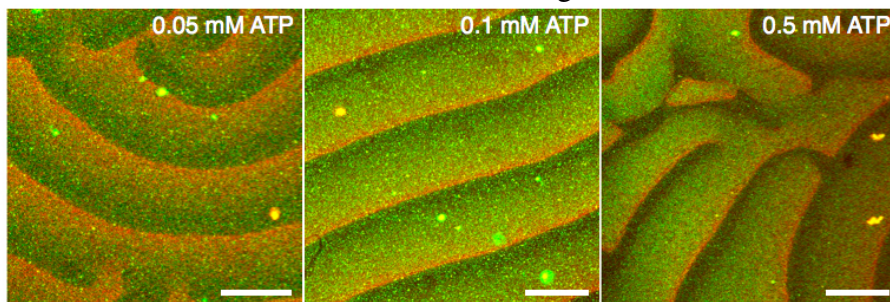
Figure S8:
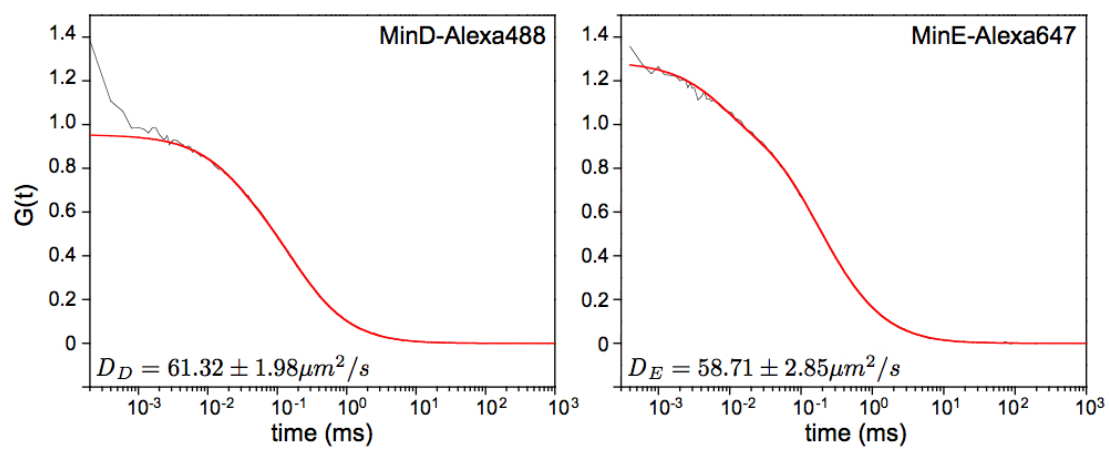
Figure S9:
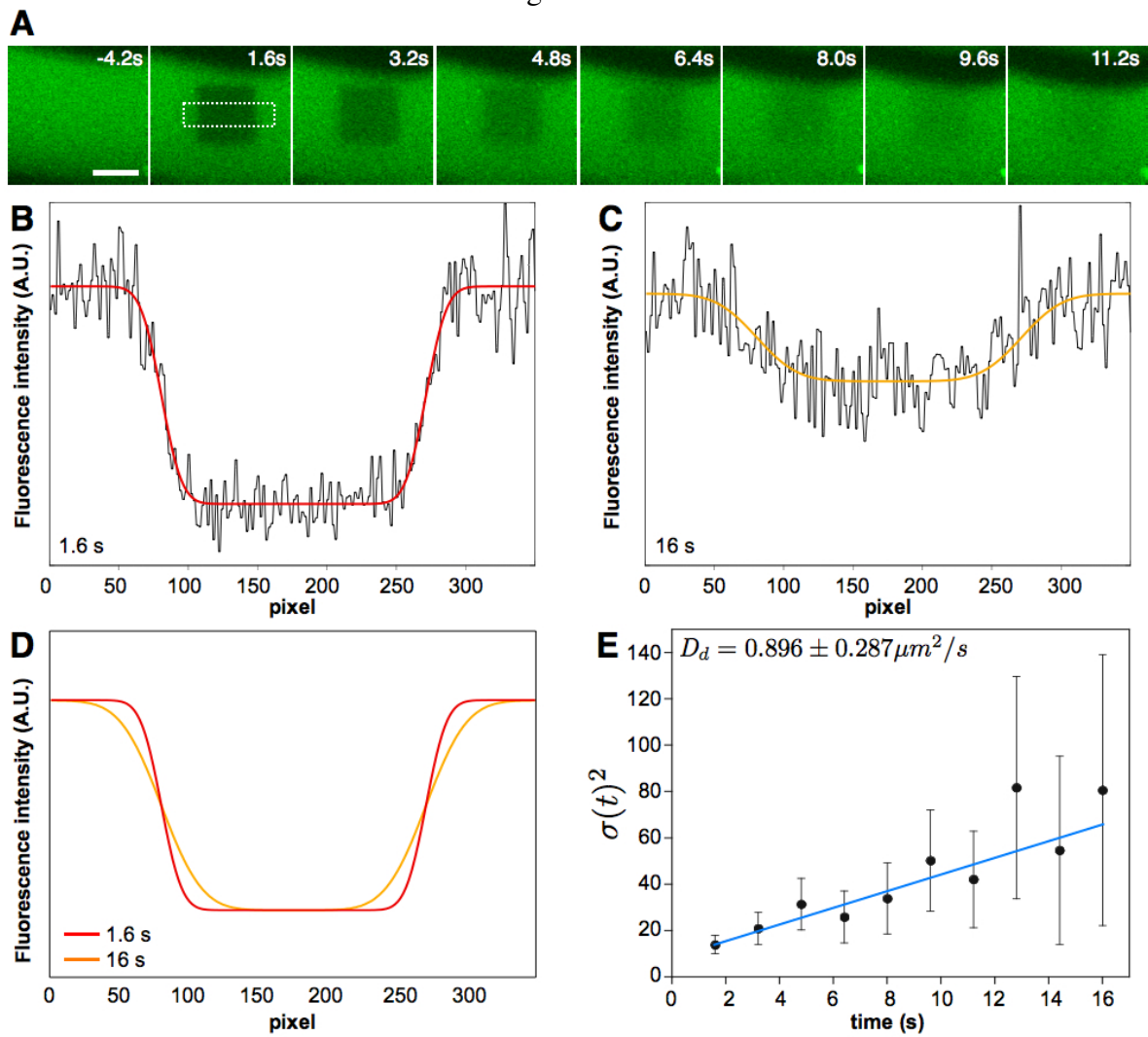
Figure S10:
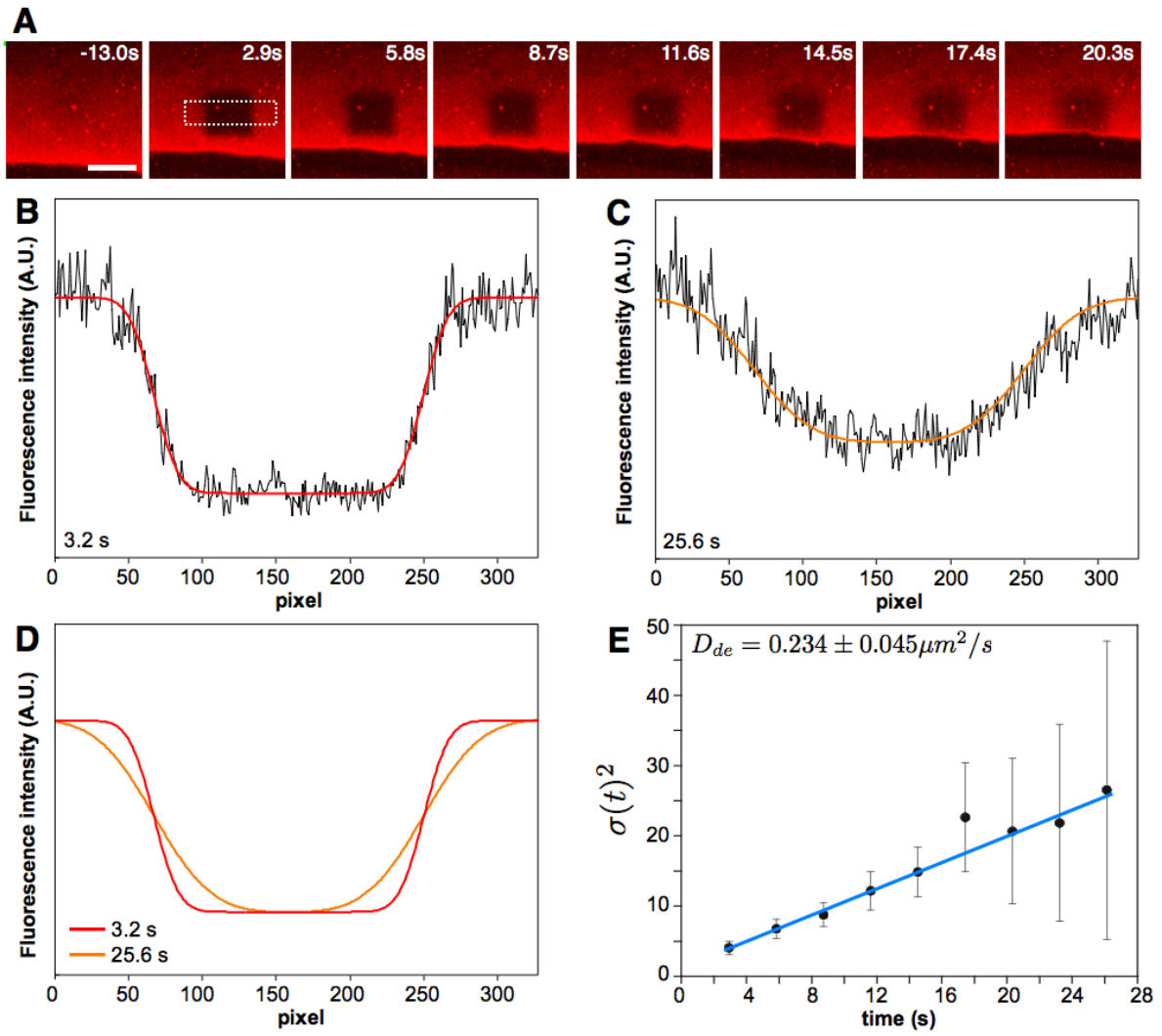
Figure S11:
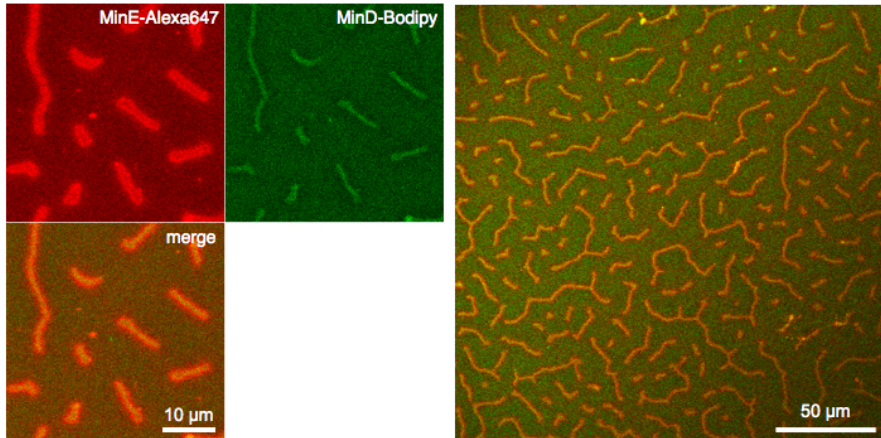
Figure S12:
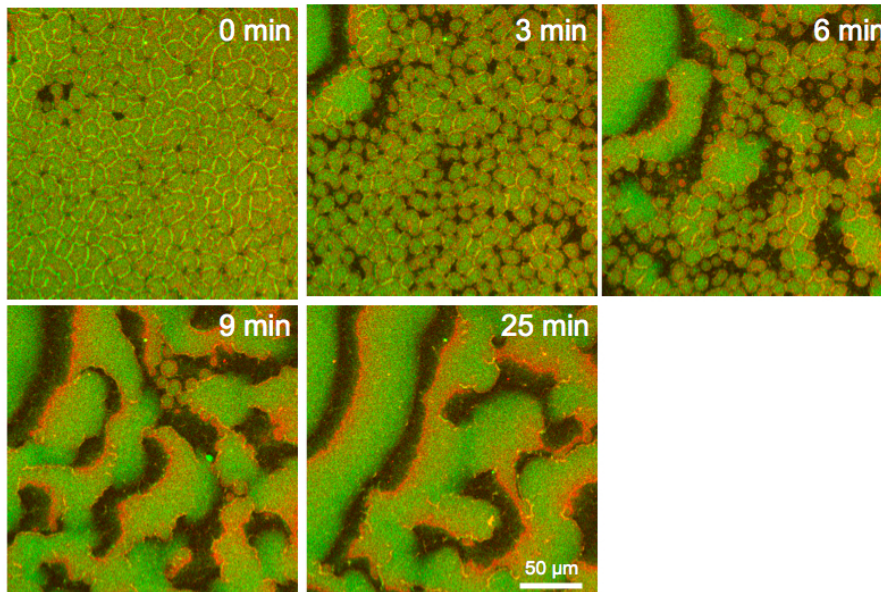
Figure S13:
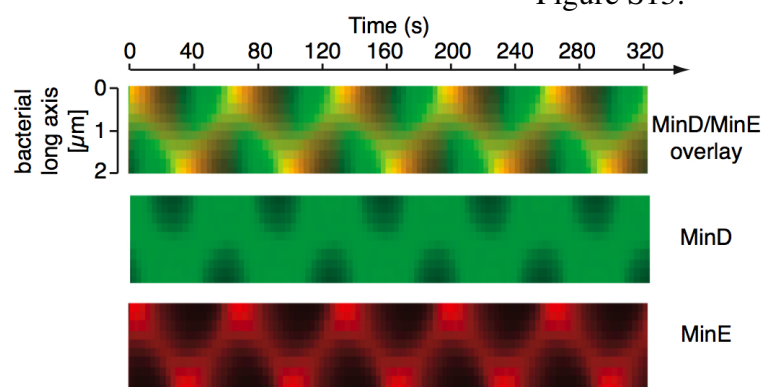
Bibliography

1. B. D. Corbin, X.-C. Yu, W. Margolin, *EMBO J* **21**, 1998 (2002).

2. D. D. Hackney, W. Jiang, *Methods Mol Biol* **164**, 65 (2001).

3. M. Merzlyakov, E. Li, K. Hristova, *Langmuir* **22**, 1247 (2006).

4. E. Haustein, P. Schwille, *Annu Rev Biophys Biomol Struct* **36**, 151 (2007).

5. K. C. Huang, Y. Meir, N. S. Wingreen, *Proc Natl Acad Sci U S A* **100**, 12724 (2003).

6. G. Meacci, K. Kruse, *Phys Biol* **2**, 89 (2005).

7. G. Meacci, *et al.*, *Phys Biol* **3**, 255 (2006).

8. L. L. Lackner, D. M. Raskin, P. A. J. de Boer, *J Bacteriol* **185**, 735 (2003).

9. G. F. King, *et al.*, *Mol Microbiol* **31**, 1161 (1999).

10. G. F. King, *et al.*, *Nat Struct Biol* **7**, 1013 (2000).

11. D. M. Raskin, P. A. de Boer, *Cell* **91**, 685 (1997).

12. K. Suefuji, R. Valluzz, D. RayChaudhuri, *Proc Natl Acad Sci U S A* **99**, 16776 (2002).

13. Z. Hu, E. P. Gogol, J. Lutkenhaus, *Proc Natl Acad Sci U S A* **99**, 6761 (2002).

14. Z. Hu, J. Lutkenhaus, *Mol Microbiol* **47**, 345 (2003).

15. H. Zhou, J. Lutkenhaus, *J Bacteriol* **185**, 4326 (2003).

16. H. Zhou, *et al.*, *J Bacteriol* **187**, 629 (2005).

17. Y.-L. Shih, T. Le, L. Rothfield, *Proc Natl Acad Sci U S A* **100**, 7865 (2003).